View Article Online / Journal Homepage / Table of Contents for this issue

Influence of the aliphatic chain length of imidazolium based ionic liquids on the surface structure

Tobias Hammer,* Manuela Reichelt and Harald Morgner

Received 17th March 2010, Accepted 28th June 2010
DOI: 10.1039/c004415f

Published on 29 July 2010. Downloaded by Michigan State University on 19/01/2016 00:56:46.

The molecular surface structure of four imidazolium based ionic liquids was studied with two surface sensitive techniques. Angle resolved neutral impact collision ion scattering spectroscopy (ARNICISS) allows us to determine elemental concentration depth profiles and to obtain information about the topography of the surface. Angle resolved X-ray photoelectron spectroscopy (ARXPS) can be used to study the chemical composition of the surface. The room temperature ionic liquids (RTILs) 1-ethyl-3-methylimidazolium [EMIM], 1-butyl-3-methylimidazolium [BMIM], 1-hexyl-3-methylimidazolium [HMIM], and 3-methyl-1-octylimidazolium [OMIM] bis(trifluoromethylsulfonyl)imide [Tf_2N] were investigated at 293 K. No evidence of surface active impurities was observed. The majority of previous studies about these RTILs with ARXPS or other surface sensitive techniques dealt only with single examples of these substances or with different combination of the anion and cation. In this present study a homologous series of the four RTILs mentioned above was investigated. This means that only the number of carbon atoms in the aliphatic chain of the cation is varied. Due to this procedure it is possible to study the influence of the chain length, which is a part of the imidazolic ring, on the composition of the surface and the surface near region. In this paper we demonstrate the potential of ARNICISS as a surface sensitive technique to study the surface structure of the RTILs. Furthermore, we combine our NICISS data with ARXPS data, to get a better comprehension of the influence of the aliphatic chain length. After the presentation of the results we develop a model of the surface structure of different RTILs. We have discovered two different surface structures that depend on the number of carbon atoms inside the aliphatic chain.

1. Introduction

Ionic liquids (ILs) are salts with melting points below 100 °C. Particular research interest is devoted to room temperature ILs (RTILs) due to their excellent properties, *e.g.*, wide temperature range of liquid state, very low vapour pressure or high heat capacity.[1,2] All these properties make them good candidates for use in many fields, especially as "green" solvents. The huge variety of possible chemical compositions allows their properties to be tailored for specific applications. A good overview of the chemical research of ILs is given in ref. 3. However, the physico-chemical behaviour of RTILs or in general ILs is still not clearly understood and needs further studies.

To investigate the influence of the composition on the surface properties it is helpful to use a homologous series, *e.g.*, the aliphatic chain length of the cation, the kind of cation or the anion. Only with the information about the influence of the cation and anion on different properties of the IL it is possible to build up the required solvent. The investigation of the liquid/vapour interface with surface sensitive methods is relevant for the understanding of surface properties and all kinds of chemical reactions at the surface, *e.g.*, electrochemical cells, phase-separable catalysis and chemical extraction processes.[4,5] In particular the knowledge of the molecular surface structure and the surface composition of liquids is important for the understanding mentioned above and the selective use for specific applications.

Usually, surface sensitive methods which are using particles like electrons or ions are applicable under high or ultra-high vacuum (UHV) conditions. This is the limiting factor for the investigation of many liquids with spectroscopic methods like neutral impact collision ion scattering spectroscopy (NICISS) or X-ray photoelectron spectroscopy (XPS). The possibility of performing vacuum based measurements on ILs due to their low vapour pressure has been discovered some years ago. Therefore, a few numbers of studies of several ILs with surface sensitive techniques,[6–11] mostly XPS, have been carried out.[12–23]

Our group is specialized on the investigation of liquid surfaces with vacuum based spectroscopic methods. In the past we have investigated the surface and the surface near region of different solvents and dissolved substances.[24–29]

In this work we combine NICISS and XPS to investigate the elemental surface composition, the elemental concentration depth profiles of the surface near region and the molecular surface structure of a homologous series of RTILs. The angle resolved mode of NICISS allows an investigation of the topology of a liquid surface and the elemental composition of the surface near region. By using angle resolved XPS it is

Wilhelm Ostwald Institute for Physical and Theoretical Chemistry, University Leipzig, Linnéstr. 2, D-04103 Leipzig, Germany. E-mail: hammer@chemie.uni-leipzig.de

 This journal is © the Owner Societies 2010

View Article Online

Published on 29 July 2010. Downloaded by Michigan State University on 19/01/2016 00:56:46.

possible to determine elemental and chemical states of the surface and the surface near region. During the discussion the results of both methods will be used to develop stepwise a model of the surface of the RTILs. The chosen substances are imidazolium based RTILs as follows: 1-ethyl-3-methylimidazolium [EMIM], 1-butyl-3-methylimidazolium [BMIM], 1-hexyl-3-methylimidazolium [HMIM], and 3-methyl-1-octylimidazolium [OMIM] bis(trifluoromethylsulfonyl)imide [Tf_2N]. While the type of anion was fixed the cation was changed by varying the alkyl chain length, permitting to study the influence of the alkyl chain length. To our knowledge, this is the first attempt to combine the two methods for investigating the surface structure of ILs.

2. Experimental section

2.1 Materials

All RTILs were purchased from Solvent Innovation GmbH or Merck Chemical Co. The origin of the ILs (CAS-no. and stated mass fraction purity) were as follows: [EMIM][Tf_2N] (174899-82-2, Solvent Innovation GmbH, 0.99); [BMIM][Tf_2N] (174899-83-3, Solvent Innovation GmbH, 0.99); [HMIM][Tf_2N] (382150-50-7, Solvent Innovation GmbH, 0.99); and [OMIM][Tf_2N] (178631-04-4, Merck Chemical Co., 0.99). An overview of the structure of all investigated RTILs is given in Table 1.

The purity of all RTIL samples was checked by using ^{1}H- and ^{13}C-NMR. In addition the water content of each sample was estimated by means of Karl Fischer Titration (METROHM Titrino plus 870). The measured water contents of the RTILs were lower than 0.1 wt% and located close to the detection limit of the coulometric Karl Fischer titration.

2.2 Sample preparation

In the following part the preparation of the liquid surfaces will be described. Generally, this preparation method is quite different from the procedure described in the literature.[10,14–17,19,22,30]

We use an *in situ* prepared liquid surface, thus avoiding contact of the surface of the RTILs with ambient air. The liquid surface is steadily refreshed and is characterized by a very short exposition time to the vacuum ($t \leq 0.2$ s).

This preparation method has been tested for the investigation of liquid surfaces,[31–34] also for RTILs.[9,35]

For generating a liquid surface as a liquid film with a thickness of several tenths of millimeter a rotating steel disk is used. This disk is partially immersed into a small reservoir filled with the liquid sample. After emerging from the reservoir the disk passes by a skimmer that removes a part of the liquid lamella. Thus, a fresh surface is created and will be hit by the ion beam. Further details of our experimental setup are published elsewhere.[36–38]

After filling the reservoir with a RTIL, the samples are inserted into the vacuum system. The chamber is pumped down until the base pressure for the vacuum system is achieved.

All measurements shown here were carried out at a temperature of 293 K that was measured with a Pt-resistance thermometer and was kept constant by using a Peltier-element.

By changing the corresponding RTIL between the measurements, the target and all other parts, which have contact to the liquid, were cleaned in an ultrasonic bath with water, 2-propanol and acetone.

In order to confirm that no impurities have contaminated the surface and affected the results, the measurements of all RTILs were repeated 2–3 times.

2.3 NICISS and ARNICISS

NICISS exploits the energy loss of helium projectiles being backscattered from soft matter targets under a fixed scattering angle of 168°. The method is used to determine elemental concentration depth profiles of the investigated liquid surfaces.

Table 1 Overview of the investigated RTILs

Structure	Name	Abbreviation
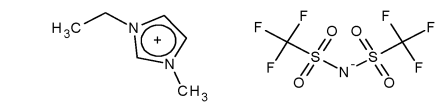	1-Ethyl-3-methylimidazolium bis(trifluoromethylsulfonyl)imide	[EMIM][Tf_2N]
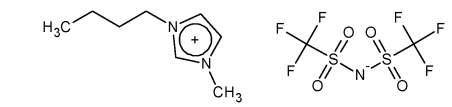	1-Butyl-3-methylimidazolium bis(trifluoromethylsulfonyl)imide	[BMIM][Tf_2N]
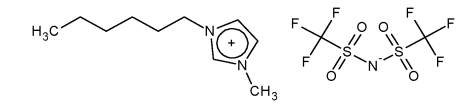	1-Hexyl-3-methylimidazolium bis(trifluoromethylsulfonyl)imide	[HMIM][Tf_2N]
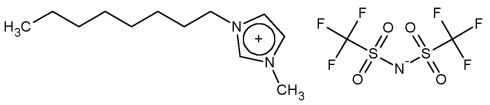	3-Methyl-1-octylimidazolium bis(trifluoromethylsulfonyl)imide	[OMIM][Tf_2N]

View Article Online

Published on 29 July 2010. Downloaded by Michigan State University on 19/01/2016 00:56:46.

The target is bombarded with a pulsed helium ion beam with a kinetic energy of several keV. During the backscattering process the He projectiles lose part of their kinetic energy according to the laws of a classical collision between two collision partners.[39] The energy transfer from projectile to target atom depends on the mass of the target atom. On their trajectory through the bulk the He projectiles suffer an additional energy loss with a magnitude proportional to the depth of the target atom. This energy loss has been calibrated with self-assembled monolayers of alkanethiolates on gold and silver single crystals.[40] The observation depth of the target atoms depends on the elemental composition of the liquid sample and is limited by the widening of the ion beam in the bulk due to small-angle scattering. Hence, the observation depth is up to 200 Å with a depth resolution far below 10 Å. The energy of the back-scattered projectiles is determined by their time-of-flight (TOF) from the target to the detector.

The main advantage of this surface sensitive method is the direct access to a concentration depth profile in comparison to ARXPS, where different assumptions and additional parameters are essential, to get a concentration depth profile.[28,32,41–43]

In the present work the kinetic energy of the projectiles was 4.5 keV. The dose of He ions was about 10^{10} ions per cm^2. Thus the damage of the surface and influence of the impinging ions on the surface structure can be neglected. During the measurements the pressure in the vacuum chamber was below 5×10^{-5} mbar.

When using the angle resolved mode of NICISS (ARNICISS) the incident angle of the ion beam is varied. Note that the scattering angle of 168° is fixed. Due to this experimental setup, the angle between the incoming helium ions and the TOF-detector is 12°. For ARNICISS measurements the target has to be aligned in such a way that the TOF distance is constant for all incident angles. Thus the rotation axis of the target and the investigation region of the liquid have to be placed directly on the surface of the rotating disk. For clarity the same angle designation like the ARXPS measurements will be used. Therefore, the observation angle is defined with respect to the surface normal. For every observation angle a laterally averaged concentration depth profile is obtained. Combining the information from different observation angles (*cf.* Fig. 1) allows developing a 3-dimensional model structure of the surface.

2.4 Data evaluation of ARNICISS

As mentioned above, the energy of the back-scattered particles is determined by their time-of-flight from the target to the detector. The TOF-spectra are composed of a structure-less recoil signal that results from sputtered hydrogen atoms and step like signals due to He projectiles being backscattered by the elements (*cf.* Fig. 2). The estimation of the concentration depth profiles is based on different complex procedures that have been described in detail in former publications.[24,25,37] Therefore, only a short statement will follow.

At first, the hydrogen recoil contribution has to be subtracted by fitting an analytical function to the TOF-spectrum. This function has to be identical to the TOF-spectrum before the onset of the heaviest element (here sulfur) and parallel to the TOF-spectrum in the bulk region of each element (short section before the onset of the next step like signal).[37] As the hydrogen recoil is conceived to be a smooth function of flight time (energy) a low order polynomial is suited for this purpose. A maximum around the carbon step is always observed. To illustrate this fact the hydrogen recoil with the described curve progression is added to Fig. 2. After subtracting the hydrogen recoil, the step like signals of the different elements are fitted with a step function that considers the energy loss of the impinging projectile, by the backscattering process and

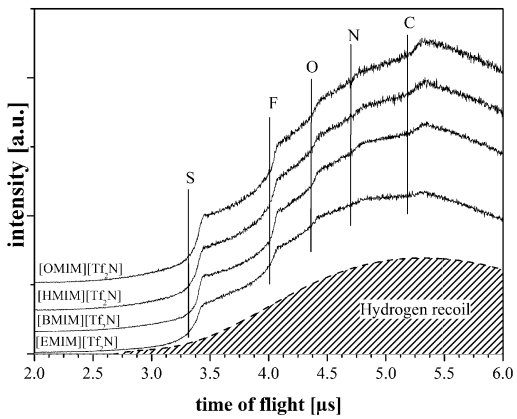

Fig. 2 NICIS time-of-flight spectra of the investigated RTILs at an observation angle of 0°. The spectra are vertically offset for clarity. Furthermore, the hydrogen recoil is shown.

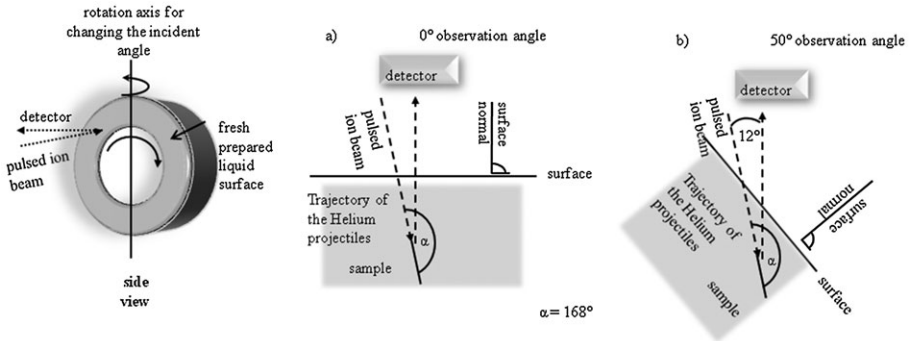

Fig. 1 Scheme of the target disk. The rotation axis of the target is placed on the surface of the rotating disk. The investigated liquid area is situated directly on the rotation axis. The scattering angle α is fixed to 168°.

 This journal is © the Owner Societies 2010

View Article Online

Published on 29 July 2010. Downloaded by Michigan State University on 19/01/2016 00:56:46.

the outgoing trajectory.[37] Note that the back-scattered projectiles from the outermost surface layer have not suffered an inelastic energy loss. For estimating the concentration depth profiles of each element, the elemental profiles on the time scale have to be converted into an energy scale which is described in detail elsewhere.[37] The depth of a target atom is estimated using the inelastic energy loss (stopping power) that means the difference of energy of a back-scattered helium projectile from the outermost surface layer and the energy of a helium projectile being back-scattered from the bulk.

The widening of the ion beam increases with increasing penetration depth into the sample matter. Thus, the time spectrum can be considered as a convolution between the spectrum and the energy profile of the ion beam as a function of depth. Hence, they can be deconvoluted by Gauss functions, whilst the beam widening in the bulk can be simulated by Gauss functions that are broadened with increasing depth of the hit target atom.[25]

2.5 XPS and ARXPS

XPS is a vacuum based standard method for surface structure investigations of solids and liquids. For this reason XPS is a useful addition to the NICISS measurements. The equipment used to perform the XPS experiments was completely manufactured by SPECS and is dimensioned for UHV conditions. This machine consists of two vacuum chambers, a main chamber and a chamber for sample preparation, which can be separated by a plate valve. The main chamber is equipped with the monochromatic Al Kα X-ray source XRC 1000 and the hemispherical analyzer PHOIBOS 100-MCD5.

The vacuum system consists of 9 turbo molecular and 3 rotary pumps with a pumping power of 60 l s^{-1} to 520 l s^{-1} and 25 m^3 h^{-1}, respectively. Furthermore, a cooling-trap can be used to remove the condensable parts of the residual vapour of the liquid. In the absence of a liquid the base pressure in the main chamber is several 10^{-9} mbar. The presence of a non-volatile sample like an IL has led to an increase of the pressure up to a value of 8×10^{-8} to 2×10^{-7} mbar. These phenomena are based on the experimental setup of the system. Before the measurement the sample is located in the preparation chamber. While the valve between the chambers is closed, the preparation chamber is pumped down and the smooth generation of the liquid film is checked. For performing the measurement the sample is transferred into the main chamber. Both chambers are connected when recording the spectra. Therefore, the increase of the pressure in the chamber is not an effect of the sample but rather of the experimental setup. These phenomena can be also observed by using a solid sample like silver.

For performing angle resolved XPS (ARXPS) investigations the target is mounted on a manipulator that permits to change the observation angle of the analyzer. The angle between incoming X-rays and photoelectron take-off direction is fixed to 55° and the electron energy analyzer radial acceptance aperture is ±6°. During the measurements presented in this work the observation angle was varied from 0° to 70° with respect to the surface normal. An increase of the angle beyond 70° as done by Lovelock *et al.*[19] or others[22,23] was not performed in order to avoid artefacts described by Baschenko *et al.* in 1991.[41,42]

Based on the construction (described in the previous part) the exposition time of the liquid film to the X-ray beam is very short (lower than 0.2 s), for which reason damage of the substance can be neglected.

The measurements were made at 293 K. This was measured with a Pt-resistance thermometer and controlled by a cryostat.

The X-ray stability of the investigated RTILs was checked with a short experiment. Therefore, the rotating disk was stopped and a survey as well as a detail spectrum of each element was recorded. After an exposition time of 1 h at 500 W source output, the procedure was repeated and between both spectra series no difference, *e.g.*, number of peaks or the form of a peak, was observed.

For the analysis of the signals, a spectrum of each element was recorded with good resolution and good counting statistics. All spectra were measured under normal emission (0°) and under observation angles of 25°, 50°, and 70° (grazing emission).

2.6 Data evaluation of ARXPS

All XPS data were recorded using the SPECS software SPECSLAB 2 (2.32). The data files were translated into the VAMAS format and evaluated by using the UNIFIT software 2008.[44]

Generally, the experimental data of the core level signal of the RTIL were fitted with a Gaussian–Lorentzian convolution function.

3. Results

3.1 ARNICISS

Fig. 2 shows NICIS spectra of the investigated RTILs at a temperature of 293 K and an observation angle of 0°. The spectra are vertically offset for clarity. Several signals corresponding to different elements can be identified. The first step like signal in the TOF-spectra can be assigned to the sulfur atoms in the anion of the RTILs at 3.36 μs. The following signals in the spectra can be assigned to fluorine (4.01 μs), oxygen (4.35 μs), nitrogen (4.7 μs), and carbon (5.12 μs). Furthermore, no evidence of impurities by other elements like silicon (3.5 μs) could be found.

To analyze the surface composition of the RTILs with NICISS, only two involved elements are needed, which are carbon and fluorine. For clarity, only the deconvoluted concentration depth profiles of [EMIM][Tf_2N] and [OMIM][Tf_2N] are shown in the following. The two other investigated RTILs show no significant different characteristics in the depth profiles, whereas [BMIM][TF_2N] is more similar to [EMIM][Tf_2N] and [HMIM][Tf_2N] is more similar to [OMIM][Tf_2N]. As expected, the step height of the carbon signal increases with the alkyl chain length.

Fig. 3 displays the carbon and fluorine depth profiles of [EMIM][Tf_2N] at several observation angles. Carbon is enriched with a maximum in a depth of 3 Å at an observation angle near the surface normal. At grazing observation geometry no significant shift into a greater depth can be noted.

View Article Online

Published on 29 July 2010. Downloaded by Michigan State University on 19/01/2016 00:56:46.

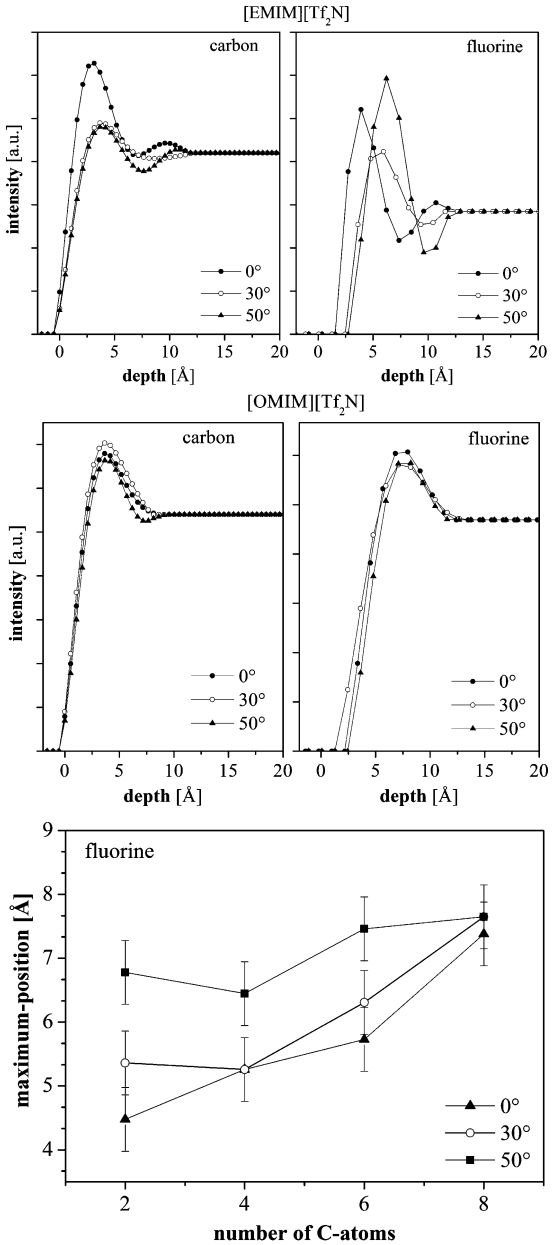

Fig. 3 Deconvoluted carbon and fluorine depth profiles of [EMIM][Tf_2N] and [OMIM][Tf_2N] at observation angles of 0°, 30°, and 50°. Furthermore, the maximum of the deconvoluted fluorine depth profiles of all investigated RTILs at observation angles of 0°, 30° and 50° is shown.

The fluorine depth profiles of [EMIM][Tf_2N] are presented in an analogous manner. In contrast to the carbon depth profiles the onset of the fluorine depth profiles starts in a greater depth. Furthermore, the maximum of the signal is shifted into a larger depth from 2 Å up to 7 Å with increasing angle of observation. A second maximum in the depth profiles of both elements can be recognized in a depth of approximately 10 Å. These phenomena result from the deconvolution procedure of the depth profiles and have no physical meaning.

The fluorine and carbon depth profiles of [OMIM][Tf_2N] are also shown in Fig. 3. For both elements no significant influence of the observation angle on the depth profile can be recognized. The carbon depth profiles of [OMIM][Tf_2N] show a similar shape with a maximum in a depth of 3 Å. The contribution of fluorine shows its maximum at 7 Å. The onset of the fluorine depth profiles starts also at a greater depth compared to the carbon depth profiles.

The lowest panel of Fig. 3 presents a summary of the deconvoluted fluorine depth profiles of all four investigated RTILs. This diagram shows the maximum of the concentration depth profile against the number of carbon atoms in the alkyl chain. The onset of the fluorine signal also changes with the increase of the chain length. At an observation angle of 0° a shift of the maximum into a greater depth with increasing chain length can be observed. Furthermore, the fluorine maximum of [EMIM][Tf_2N] shows a significant shift into a greater depth with increasing observation angle. This effect can be also observed for [BMIM][Tf_2N] and [HMIM][Tf_2N]. In contrast, [OMIM][Tf_2N] shows no shift of the maximum position when varying the geometry.

3.2 ARXPS

The survey XP-spectrum of [OMIM][Tf_2N] at 0° take-off angle is displayed in Fig. 4. All characteristic core level signals of the substance can be identified.

Furthermore, the overview scan suggests a closed liquid film, because no signal of the substrate (stainless steel) was found.

Also no evidence of impurities of other elements like silicon was recognized. The fluorine 1s core level spectrum of each RTIL exhibits only one peak at a binding energy (B.E.) of 688.9 eV. These results agree with the typical B.E. of fluorine in a CF_3-group.[15] The oxygen 1s core level also shows only one signal at 532.7 eV B.E., which can be assigned to the SO_2-group of the anion. Furthermore, the sulfur 2p core level was found at 168.8 eV B.E. The spectrum corresponds to two components due to the contribution of $2p_{\frac{1}{2}}$ (170 eV) and $2p_{\frac{3}{2}}$ (168.8 eV). This signal can be referred to sulfur in the bis(trifluoromethylsulfonyl)imide anion.

By using the signals of carbon and nitrogen, it is possible to get information about the composition of the surface and the surface near region in an elementary way. For clarity, only the

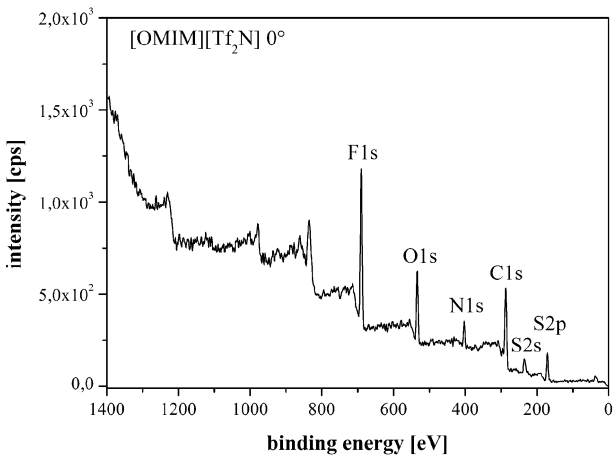

Fig. 4 Survey XP-spectrum of [OMIM][Tf_2N] at a take-off angle of 0°.

 This journal is © the Owner Societies 2010

View Article Online

Published on 29 July 2010. Downloaded by Michigan State University on 19/01/2016 00:56:46.

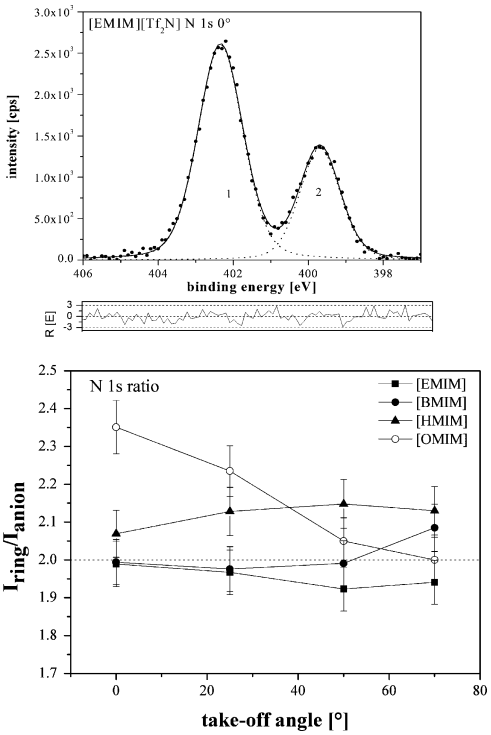

Fig. 5 The nitrogen 1s core level XPS spectrum of [EMIM][Tf_2N]. The peaks were assigned to two different species: (1) imidazolic ring C–N–C and (2) imide of the anion. The spectrum was recorded at 0° take-off angle. The filled circles represent the experimental data after the background subtraction. The fitting functions are described by the dotted lines and the resulting fit is shown as solid line. Additionally, the residual R[E] is shown. The lower graph shows the nitrogen ratio of ring to anion versus the take-off angle of all investigated RTILs.

results from the signals of carbon and nitrogen are shown and discussed, but the results of the other compounds of the RTILs support the discussed observations and interpretations in the following part. Due to the fact that carbon and nitrogen appear in the cation and the anion no additional assumption must be used to characterize the surface and the surface near area of the corresponding RTIL. Furthermore, the signals of fluorine, oxygen, and sulfur are also suited to get this information.

In Fig. 5 the N 1s core level spectrum with curve fitting components of [EMIM][Tf_2N] at 0° take-off angle is displayed. The first peak of the N 1s core level is located at 402.1 eV B.E. and can be assigned to the nitrogen atoms in the imidazolic ring.[45] The peak at 399.5 eV B.E. can be attributed to the imide nitrogen of the anion. For fitting the signals a fixed FWHM of 1.6 eV was used.

Fig. 5 shows the ratio of the N 1s core level of cation to anion. Due to the composition, the stoichiometric ratio of nitrogen atoms does not change by varying the alkyl chain and is always 2 : 1 between cation and anion. The experimental atomic ratio between both nitrogen species appears to depend on the length of the aliphatic chain and on the take-off angle. All determined ratios are listed in Table 2. At normal emission the RTILs with a shorter aliphatic chain show the same ratio as predicted by stoichiometry.

The ratio for [EMIM][Tf_2N] does not change significantly with the observation angle. For [BMIM][Tf_2N] a smooth increase of the intensity of the anion can be observed. [HMIM][Tf_2N] shows a comparable curve shape like [BMIM][Tf_2N], but the experimental ratio between both ions is higher than the stoichiometric ratio. A reversed angular dependence can be observed in the case of [OMIM][Tf_2N].

For carbon five different species are identified in the C 1s core level spectra as shown in Fig. 6. The spectrum of the C 1s core level of [EMIM][Tf_2N] at 0° take-off angle is displayed in Fig. 6. The first peak at the highest B.E. is located at 293.1 eV and can be attributed to the CF_3-group of the anion.[13] All carbon species were fitted with a Gaussian–Lorentzian function with a FHWM of 1.3 eV, respectively. The peak at the lowest B.E. (285.1 eV) originates from the aliphatic carbon of the alkyl chain. At a B.E. of 288.0 eV and 287.4 eV two other carbon species are located and can be assigned to the

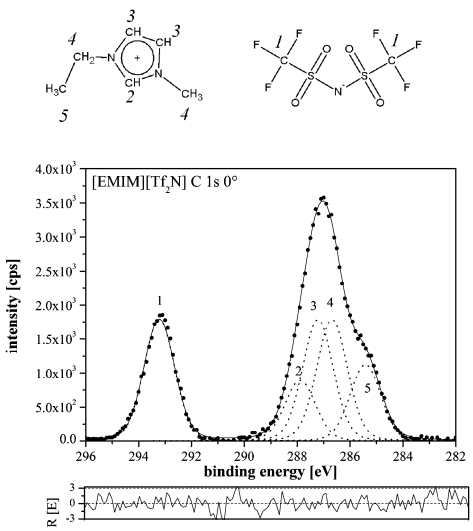

Fig. 6 Using the example of [EMIM][Tf_2N], the assignment of the five different carbon species is as follows: (1) CF_3-group, (2) imidazolic N–C–N, (3) imidazolic C–C*–N–, (4) C–N aliphatic and (5) C aliphatic. This declaration is valid for all RTILs presented here. Also the carbon 1s core level XP spectra of [EMIM][Tf_2N] at a take-off angle of 0°, *i.e.*, close to the surface normal is shown. The filled circles represent the experimental data after the background subtraction. The fitting functions are described by the dotted lines and the resulting fit is shown as solid line. Additionally, the residual R[E] is shown.

Table 2 Experimental ratio of the N 1s core level signal between the cation and the anion. The stoichiometrical values are given in brackets

Angle/°	[EMIM][Tf_2N] (2)	[BMIM][Tf_2N] (2)	[HMIM][Tf_2N] (2)	[OMIM][Tf_2N] (2)
0	1.99	1.99	2.07	2.35
25	1.97	1.97	2.13	2.23
50	1.92	1.99	2.15	2.05
70	1.94	2.08	2.13	2.02

View Article Online

Published on 29 July 2010. Downloaded by Michigan State University on 19/01/2016 00:56:46.

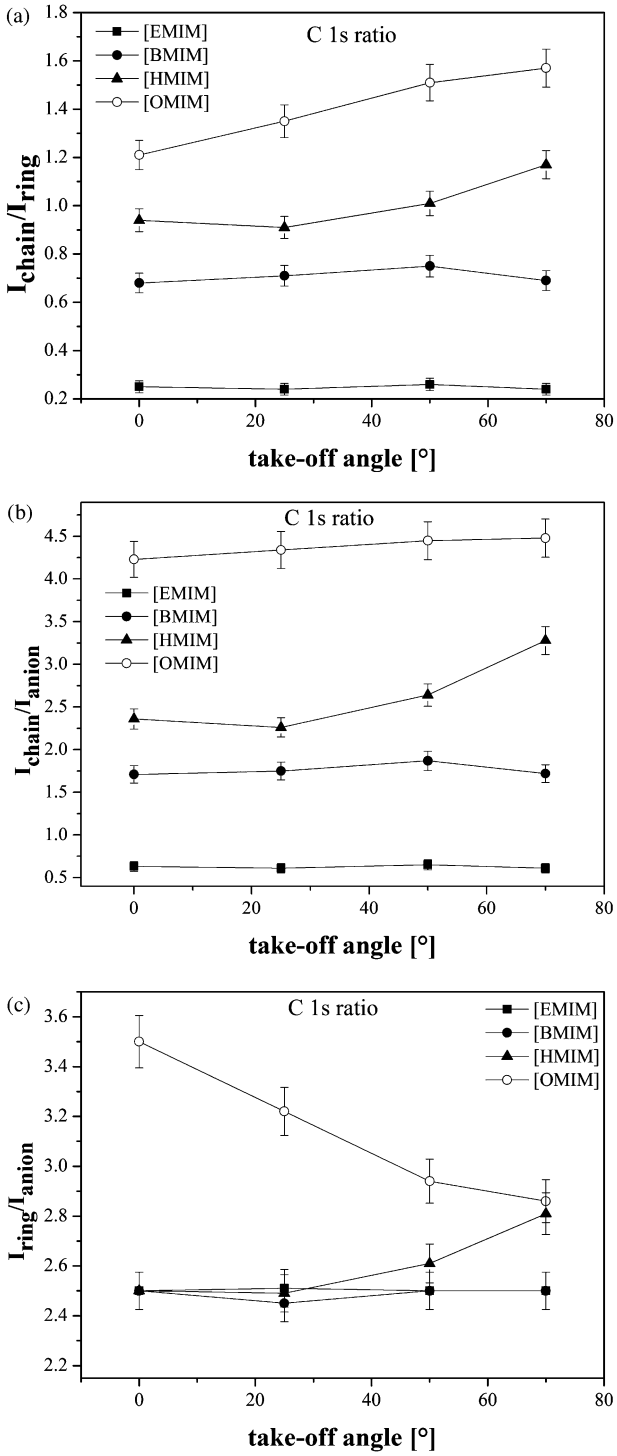

Fig. 7 Carbon ratio of (a) chain to ring ($C_5/(C_4 + C_3 + C_2)$), (b) chain to anion (C_5/C_1) and (c) imidazolic ring to anion ($(C_2 + C_3 + C_4)/C_1$) *versus* the take-off angle of all investigated RTILs.

carbon atoms in the imidazolic ring. At a B.E. of 286.7 eV one more species of carbon is observed. This signal can be referred to the two carbon atoms in the alkyl chains that are directly bonded to the nitrogen of the imidazolic ring.

Furthermore, an individual high energy shift between the first carbon species and the other four can be recognized. Caporali and coworkers[15] have also obtained such a high energy shift.

Some experimental ratios of different carbon species will be shown in the following. The ratio between the signal of the aliphatic chain (C_5) and the sum of the ring signal ($C_2 + C_3 + C_4$) is displayed in Fig. 7a. In the case of [EMIM][Tf_2N] and [BMIM][Tf_2N] the ratio does not change with increasing take-off angle. [HMIM][Tf_2N] shows an increase of the aliphatic part of the carbon signal between 25° and 70° take-off angle. This effect was also observed for [OMIM][Tf_2N] that shows a continuous increase of the signal of the aliphatic chain. Further the RTILs with longer aliphatic chain show a substoichiometric behavior at normal emission angle (0°). In contrast the [EMIM][Tf_2N] and [BMIM][Tf_2N] show a hyperstoichiometric behavior at a take-off angle parallel to the surface normal (0°). All resulting experimental ratios are listed in Table 3.

Fig. 7b shows the ratio of the aliphatic chain to the signal of the CF_3-group (C_1) of the anion (*cf.* Table 4). For [EMIM][Tf_2N] and [BMIM][TF_2N] no significant dependence of the ratio on the take-off angle was observed.

The two other RTILs possess an increase of the ratio between aliphatic chain and anion at higher emission angles. This effect is more significant for [HMIM][Tf_2N] than for [OMIM][Tf_2N].

The ratio of the intensities for the imidazolic ring ($C_2 + C_3 + C_4$) and the anion (C_1) is shown in Fig. 7c. [EMIM][Tf_2N] and [BMIM][Tf_2N] show a good agreement with the expected ratio of 2.5 which hardly varies with the take-off angle. [HMIM][Tf_2N] shows also a good correlation to the expected ratio at normal emission (0°) but a smooth increase of the amount of the imidazolic ring with increasing electron take-off angle can be observed (Table 5). However, in the case of [OMIM][Tf_2N] a higher amount of the imidazolic ring at normal emission can be observed. In addition, the part of the ring of [OMIM][Tf_2N] decreases with increasing take-off angle.

Fig. 8 shows the high resolution C 1s core level spectra of all four investigated RTILs at normal emission and also at grazing take-off angle (70°). In some C 1s spectra a smooth intensity rising near 290 eV B.E. can be recognized. Note that this phenomena cannot be observed in all spectra during a measurement series. In case of an additional surface active carbon species (impurity) this signal should increase significantly at high take-off angles and should be always present. Therefore, an effect of a surface active impurity can be neglected.

Table 3 Experimental ratio of the C 1s core level signal between the aliphatic chain (C5) and the ring (C4 + C3 + C2). The stoichiometrical values are given in brackets

Angle/°	[EMIM][Tf_2N] (0.2)	[BMIM][Tf_2N] (0.6)	[HMIM][Tf_2N] (1)	[OMIM][Tf_2N] (1.4)
0	0.25	0.68	0.94	1.21
25	0.24	0.71	0.91	1.35
50	0.26	0.75	1.01	1.51
70	0.24	0.69	1.17	1.57

 This journal is © the Owner Societies 2010

View Article Online

Published on 29 July 2010. Downloaded by Michigan State University on 19/01/2016 00:56:46.

Table 4 Experimental ratio of the C 1s core level signal between the aliphatic chain (C5) and the anion (C1). The stoichiometrical values are given in brackets

Angle/°	[EMIM][Tf_2N] (0.5)	[BMIM][Tf_2N] (1.5)	[HMIM][Tf_2N] (2.5)	[OMIM][Tf_2N] (3.5)
0	0.63	1.71	2.36	4.23
25	0.61	1.75	2.26	4.34
50	0.65	1.87	2.64	4.45
70	0.61	1.72	3.28	4.48

Table 5 Experimental ratio of the C 1s core level signal between the ring (C4 + C3 + C2) and the anion (C1). The stoichiometrical values are given in brackets

Angle/°	[EMIM][Tf_2N] (2.5)	[BMIM][Tf_2N] (2.5)	[HMIM][Tf_2N] (2.5)	[OMIM][Tf_2N] (2.5)
0	2.50	2.50	2.50	3.50
25	2.51	2.45	2.49	3.22
50	2.50	2.50	2.61	2.94
70	2.50	2.50	2.81	2.86

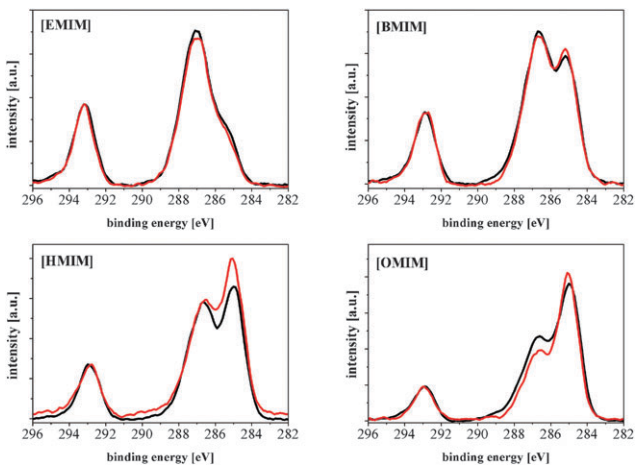

Fig. 8 High resolution spectra of the C 1s core level of all investigated RTILs obtained at electron take-off angles of 0° (black lines) and 70° (red lines), respectively. Both spectra of each RTIL are normalized to the intensity of the CF_3-group (C_1) for clarity.

4. Discussion

The discussion starts with the interpretation of the data of [OMIM][Tf_2N] as an example of a long-chain RTIL and continues with the results of [EMIM][Tf_2N] as an example of a RTIL with a short aliphatic chain. In both cases the results of the two different surface sensitive techniques are used to develop stepwise a model of the corresponding surface structure. The amount of carbon at the surface in the case of [OMIM][Tf_2N] is much larger than for [EMIM][Tf_2N]. This effect results from the surface activity of the long aliphatic chain of the cation of [OMIM][Tf_2N]. The shape of the carbon depth profile of [OMIM][Tf_2N] does not change with the observation angle. Therefore, the trajectories of the helium projectiles show no dependence on the observation angle. Due to these results it can be concluded that the trajectory through the material, which is penetrated by the projectiles, is always the same. This can be explained with an average spherical distribution of carbon atoms at the surface and the surface near region.

At an observation angle of 0° the maximum of the carbon enrichment of [OMIM][Tf_2N] is located in a depth of 3 Å (*cf.* Fig. 3). Compared with fluorine that shows its maximum at 7 Å, the carbon enrichment is closer to the surface. Due to the effect of the spherical contribution of carbon atoms at the surface fluorine must be covered by carbon. This fact is supported by the onset of the fluorine depth profile in a greater depth compared to carbon. However, no shift of the fluorine maximum can be recognized at grazing observation angle. That means that the trajectories of the projectiles are the same like the ones at 0° observation angle. Thus, the surface consists mainly of spherically distributed carbon atoms with fluorine in its center. The ratio of the aliphatic chain to the imidazolic ring of the C 1s core level signals of the XP spectra shows two different trends (*cf.* Fig. 7a). The first one is characterized by a smooth increase of the intensity of the aliphatic chain for [HMIM][Tf_2N] and [OMIM][Tf_2N] with increasing electron take-off angle. This behavior of the intensity suggests an enrichment of the aliphatic chain at the surface. These results are supported by the ratio of the aliphatic chain to the CF_3-group of the anion (Fig. 7b). Generally, the RTILs with longer aliphatic chains show a higher ratio of these carbon species at grazing observation angle. Due to these results a higher amount of the aliphatic chain on the surface can be inferred. This fact corresponds to the carbon and fluorine depth profiles of the NICIS spectra of [OMIM][Tf_2N]. This observation is not surprising, because the unpolar chain is very surface active in a polar medium, *i.e.*, the bulk phase of the RTIL.

Based on the surface enrichment of the aliphatic chain, the distribution of the other parts of the cation as well as the anion will be changed. This influence can be seen in the ratio between the imidazolic ring and the anion (*cf.* Fig. 5 and 7c). In Fig. 7c the ratio of the C 1s core levels between both ions shows different trends. [HMIM][Tf_2N] shows an increase of the ratio with increase of the take-off angle.

This effect can also be found in the N 1s core level (see Fig. 5). In contrast, [OMIM][Tf_2N] shows an opposed curve shape, since the ratio decreases with increasing take-off angle. This behavior can be noticed in both cases for the ratio of C1 s (Fig. 7) and the N 1s core level (Fig. 5). That means that at

View Article Online

Published on 29 July 2010. Downloaded by Michigan State University on 19/01/2016 00:56:46.

normal emission the amount of the anion is too low compared to the stoichiometric ratio in the case of [OMIM][Tf_2N]. For a higher take-off angle the ratio will be normalized. Therefore, the anion must be covered by other parts of the RTIL, *e.g.*, by the aliphatic chain of the cation. As mentioned above this result is supported by the NICISS data that have shown a spherical distribution of carbon with fluorine in its center. The data show also that this covering is limited to the anion, because this effect cannot be found in the intensity ratio of the alkyl chain to the imidazolic ring (*cf.* Fig. 7a). For [OMIM][Tf_2N] and a take-off angle of 0° a higher amount of the carbon species of the imidazolic ring can be observed. With increasing surface sensitivity due to the variation of the electron take-off angle the signal of the ring decreases. [HMIM][Tf_2N] shows also a higher contribution of the imidazolic ring for normal emission (0°). Therefore, the ring appears covered by aliphatic carbon only at a grazing take-off angle during the XPS measurements. This phenomenon is supported by the smooth increase of the amount of aliphatic carbon in the spectra at a grazing angle. Hence, a ring position in a local valley can be inferred. The higher amount of the ring signal at normal emission (*cf.* Fig. 7a) can be explained by a self-covering effect of the aliphatic chain, *i.e.*, due to the spherical distribution of the aliphatic chain in the case of [OMIM][Tf_2N] a part of the aliphatic carbon atoms will be covered by other aliphatic carbon atoms. However, this covering effect and the resulting higher signal of aliphatic carbon near the surface can be observed only for RTILs with long alkyl chains. Therefore, only [HMIM][Tf_2N] and [OMIM][Tf_2N] show a significant enrichment of this carbon species at the surface. At this point, let us summarize the results of the investigation of RTILs with longer aliphatic chains and develop a picture of the surface.

With ARNICISS measurements we found a spherical distribution of carbon atoms at the surface. This species belongs to the aliphatic chain, based on the ARXPS results. For a better visualization of these results, a corresponding picture of the surface of [OMIM][Tf_2N] is shown in Fig. 9. The picture shows a spherical distribution of the alkyl chain at the surface. This alkyl chain forms a spherical cap with the $[Tf_2N]^-$ anions in the center of the spherical arrangement. Furthermore, the imidazolic rings are arranged in local valleys, which are surrounded by spherical caps of alkyl chains. Lovelock *et al.* have also found an enrichment of the aliphatic chain by studying corresponding RTILs by ARXPS.[19] Computer simulations of this type of RTIL have pointed out an enrichment of the alkyl chain at the outermost layer. Sanmartín Pensado *et al.* have shown by Molecular Dynamic (MD) calculation a trend of the chain of [HMIM][Tf_2N] towards the vacuum, with the imidazolic ring placed more into the liquid bulk phase.[46] Iwahashi *et al.* investigated RTILs which contain also the $[Tf_2N]^-$ anion with Metastable Induced Electron Spectroscopy (MIES).[10] In case of RTILs with a long aliphatic chain like [OMIM][Tf_2N], they found that the outermost surface is covered by an alkyl chain layer which conceals the anion. These studies support a covering of the surface by long alkyl chain and a trend of the imidazolic ring closer to the bulk, *i.e.*, in a local valley. Furthermore, the ARNICISS results show a higher amount of fluorine in the center of the spherically distributed carbon atoms of the alkyl chain. An orientation of the alkyl chain towards the vacuum, *i.e.*, an orientation parallel to the surface normal, is unlikely. In a previous study Morgner *et al.* have shown with MIES that the aliphatic chains of a sodium-oleate (NaOl) lie flat on a liquid surface up to the completion of a closed layer.[47] Only after the completion of this layer the NaOl molecules begin to reorient into an upright position which allows more molecules to be accommodated at the surface. Due to the sterical composition of the investigated RTILs and the high flexibility of the alkyl chain, the amount of aliphatic chains is too low to feature this upright position.

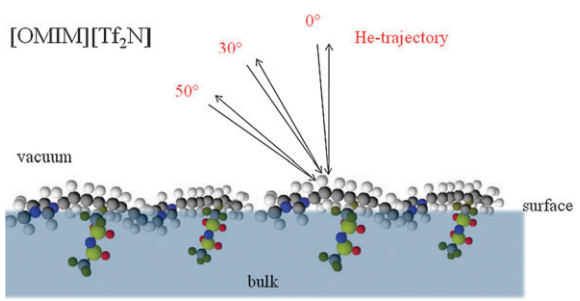

Fig. 9 Cross-section of a 3-dimensional schematic picture of the surface structure of [OMIM][Tf_2N] resulting from the evaluation of the NICISS and the XPS data. Furthermore, the trajectories of the helium projectiles of some ARNICISS measurements are shown.

The carbon and fluorine depth profiles of [EMIM][Tf_2N] show clearly that fluorine is not isolated at the topmost surface layer (*cf.* Fig. 3). By varying the observation angle to higher observation angle (50°) the position of the fluorine maximum is shifted into a greater depth. In case of an enrichment of the anion, the depth profile of fluorine has to show a significant increase of the signal and also no shift to a greater depth. However, the opposite condition is the case (*cf.* Fig. 3). This means that the helium projectiles must cross a longer distance until they hit a fluorine atom. In contrast, the shift of the maximum of the carbon signals is only slight. This result suggests a structure with homogeneously distributed carbon, *e.g.*, of the cation, near the surface and a position of the fluorine containing anion in a greater depth, *i.e.*, in a local valley.

The ratio of the aliphatic chain to the imidazolic ring of the C 1s core level of RTILs with a shorter aliphatic chain (*cf.* Fig. 7a) like [EMIM][Tf_2N] and [BMIM][Tf_2N] shows a constant value for all take-off angles. These results are supported by the ratio of the aliphatic chain to the CF_3-group of the anion (Fig. 7b). Therefore, a homogeneous distribution of the alkyl carbons of the cation at the surface near region can be concluded. In comparison to the stoichiometrical ratio a deviation can be observed. In both cases the C1 s ratio shows a higher intensity of the aliphatic chain (C_5) than the stoichiometrical ratio has predicted. If adsorbed hydrocarbons or other impurities would be located at the surface, the intensity would increase dramatically at grazing take-off angle. However, such an effect is not found. Therefore, an offset of the aliphatic chain signal due to impurities can be neglected. Furthermore, a covering of homogeneously distributed carbon species of the cation is possible. In Fig. 7c the ratio of the C 1s core levels

 This journal is © the Owner Societies 2010

View Article Online

Published on 29 July 2010. Downloaded by Michigan State University on 19/01/2016 00:56:46.

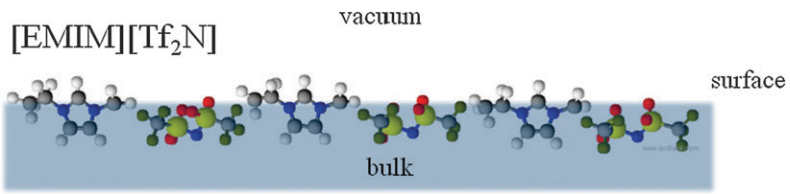

Fig. 10 Cross-section of a 3-dimensional schematic picture of the surface structure of [EMIM][Tf_2N] resulting from the evaluation of the NICISS and the XPS data.

between both ions of [EMIM][Tf_2N] and [BMIM][Tf_2N] shows a weak value with a fluctuation observed within the error bars. The same result can be concluded from the ratio of the intensity of the N 1s core level between cation and anion (*cf*. Fig. 5). In comparison to the C 1s the N 1s core level signals show a stoichiometrical ratio of the ions at all different electron take-off angles.

At this point, we want to develop a 3-dimensional model for [EMIM][Tf_2N] as an example for a RTIL with a short aliphatic chain. Concerning the discussed results a cartoon picture of the surface structure is shown in Fig. 10. The ARNICISS results show no evidence of a surface enrichment of the anion but rather a shift into the depth. Furthermore, ARNICISS measurements have shown that the carbon containing parts of the RTIL follow a homogeneous distribution. Therefore, a homogeneous distribution of both ions on the surface and the surface near area will be suggested. This fact is also suggested by the ratio of the anion to the cation (*cf*. Fig. 5 and 7c). Günster *et al*. have studied the same RTIL by time-of-flight-secondary ion mass spectroscopy (TOF-SIMS).[48] One of the results of this study was the conclusion that the CF_3-group of the anion is not isolated on the liquid surface and the small alkyl chains of the imidazolic ring are exposed to the vacuum. Iwahashi *et al*. found an orientation of the nonpolar parts of the corresponding RTIL pointing away from the bulk in the case of a very short aliphatic chain.[10] This observation is also supported by our ARXPS results, especially by the ratio of the aliphatic chain to the anion (*cf*. Fig. 7b) and also to the imidazolic ring (*cf*. Fig. 7a). Due to the limited flexibility of the chain, the anion cannot be covered by them. Therefore, the anion is also exposed to the vacuum and is visible for an observation close to the surface normal. Computer simulations of comparable RTILs have indicated that the anions and rings can be seen from the vacuum. Further, the simulations of Lynden-Bell and Del Pópolo[49] have shown that the anions do not penetrate the layer of ring and aliphatic chain, but rather that the anions are located in local valleys, *i.e*., in a larger depth.

5. Summary

We have investigated the surface structure and the elemental composition of a homologous series of four RTILs, *i.e*., [EMIM][Tf_2N], [BMIM][Tf_2N], [HMIM][Tf_2N], and [OMIM][Tf_2N]. Angle resolved neutral impact collision ion scattering spectroscopy and angle resolved X-ray photoelectron spectroscopy were used to investigate the surface and the surface near region of these liquids. Two different surface structures, depending on the chain length of the investigated RTILs, were found. In the case of a short aliphatic chain, *e.g*., [EMIM][Tf_2N] and [BMIM][Tf_2N], no enrichment or high level of orientation of the aliphatic chain of the cation into the vacuum was observed. For RTILs with a longer aliphatic chain like [OMIM][Tf_2N] a different surface structure was identified. The long alkyl chain of the imidazolic ring covers the anion, *i.e*., no fluorine is located directly at the surface. Additionally, this chain shows a spherical distribution with an anion in its center. Further, the imidazolic ring is arranged in a local valley that is surrounded by the spherically distributed aliphatic chains of other [OMIM][Tf_2N] molecules.

Acknowledgements

The financial support from the Deutsche Forschungsgemeinschaft priority program "Ionic Liquids" (SPP 1191) is acknowledged.

References

1 P. Wasserscheid and W. Keim, *Angew. Chem., Int. Ed.*, 2000, **112**, 3926–3945.
2 F. Endres and S. Z. El Abedin, *Phys. Chem. Chem. Phys.*, 2006, **8**, 2101.
3 R. D. Rogers and G. A. Voth, *Acc. Chem. Res.*, 2007, **40**, 1077–1078.
4 A. Riisager, P. Wasserscheid, R. van Hal and R. Fehrmann, *J. Catal.*, 2003, **219**, 452.
5 S. Baldelli, *Acc. Chem. Res.*, 2008, **41**, 421.
6 S. Krischok, M. Eremtchenko, M. Himmerlich, P. Lorenz, J. Uhlig, A. Neumann, R. Ottking, W. J. D. Beenken, O. Hofft, S. Bahr, V. Kempter and J. A. Schaefer, *J. Phys. Chem. B*, 2007, **111**, 4801–4806.
7 S. Baldelli, *J. Phys. Chem. B*, 2003, **107**, 6148–6152.
8 S. Baldelli, *J. Phys. Chem. B*, 2005, **109**, 13049–13051.
9 K. Nakajima, A. Ohno, M. Suzuki and K. Kimura, *Nucl. Instrum. Methods Phys. Res., Sect. B*, 2009, **267**, 605–609.
10 T. Iwahashi, T. Nishi, H. Yamane, T. Miyamae, K. Kanai, K. Seki, D. Kim and Y. Ouchi, *J. Phys. Chem. C*, 2009, **113**, 19237–19243.
11 H. Hashimoto, A. Ohno, K. Nakajima, M. Suzuki, H. Tsuji and K. Kimura, *Surf. Sci.*, 2010, **604**, 464–469.
12 O. Höfft, S. Bahr, M. Himmerlich, S. Krischok, J. A. Schaefer and V. Kempter, *Langmuir*, 2006, **22**, 7120–7123.
13 E. F. Smith, F. J. M. Rutten, I. J. Villar-Garcia, D. Briggs and P. Licence, *Langmuir*, 2006, **22**, 9386–9392.
14 O. Höfft, S. Bahr and V. Kempter, *Langmuir*, 2008, **24**, 11562–11566.
15 S. Caporali, U. Bardi and A. Lavacchi, *J. Electron Spectrosc. Relat. Phenom.*, 2006, **151**, 4–8.
16 O. Höfft, S. Bahr and V. Kempter, *Anal. Sci.*, 2008, **24**, 1273–1277.
17 C. Kolbeck, T. Cremer, K. R. J. Lovelock, N. Paape, P. S. Schulz, P. Wasserscheid, F. Maier and H. P. Steinrück, *J. Phys. Chem. B*, 2009, **113**, 8682–8688.
18 C. Kolbeck, M. Killian, F. Maier, N. Paape, P. Wasserscheid and H.-P. Steinrück, *Langmuir*, 2008, **24**, 9500–9507.

View Article Online

Published on 29 July 2010. Downloaded by Michigan State University on 19/01/2016 00:56:46.

19 K. R. J. Lovelock, C. Kolbeck, T. Cremer, N. Paape, P. S. Schulz, P. Wasserscheid, F. Maier and H. P. Steinrück, *J. Phys. Chem. B*, 2009, **113**, 2854–2864.
20 J. M. Gottfried, F. Maier, J. Rossa, D. Gerhard, P. S. Schulz, P. Wasserscheid and H.-P. Steinrück, *Z. Phys. Chem.*, 2006, **220**, 1439–1453.
21 F. Maier, J. M. Gottfried, J. Rossa, D. Gerhard, P. S. Schulz, W. Schwieger, P. Wasserscheid and H.-P. Steinrück, *Angew. Chem., Int. Ed.*, 2006, **45**, 7778–7780.
22 V. Lockett, R. Sedev, C. Bassell and J. Ralston, *Phys. Chem. Chem. Phys.*, 2008, **10**, 1330–1335.
23 F. Maier, T. Cremer, C. Kolbeck, K. R. J. Lovelock, N. Paape, P. S. Schulz, P. Wasserscheid and H. P. Steinruck, *Phys. Chem. Chem. Phys.*, 2010, **12**, 1905–1915.
24 G. Andersson, *Phys. Chem. Chem. Phys.*, 2005, **7**, 2942–2947.
25 G. Andersson, H. Morgner and H. Pohl, *Phys. Rev. A: At., Mol., Opt. Phys.*, 2008, **78**, 032904.
26 T. Krebs, G. Andersson and H. Morgner, *J. Phys. Chem. B*, 2006, **110**, 24015–24020.
27 T. Krebs, G. Andersson and H. Morgner, *Chem. Phys.*, 2007, **340**, 181–186.
28 G. Andersson, T. Krebs and H. Morgner, *Phys. Chem. Chem. Phys.*, 2005, **7**, 2948–2954.
29 H. Pohl, T. Krebs and H. Morgner, *Langmuir*, 2009, **26**, 2473–2476.
30 S. Caporali, U. Bardi and A. Lavacchi, *J. Electron Spectrosc. Relat. Phenom.*, 2006, **151**, 4.
31 R. Moberg, F. Bokman, O. Bohman and H. O. G. Siegbahn, *J. Chem. Phys.*, 1991, **94**, 5226–5232.
32 O. A. Baschenko, F. Bökman, O. Bohman and H. O. G. Siegbahn, *J. Electron Spectrosc. Relat. Phenom.*, 1993, **62**, 317–334.
33 F. B. R. Moberg, O. Bohman and H. O. G. Siegbahn, *J. Am. Chem. Soc.*, 1991, **113**, 3663–3667.
34 F. Bökman, O. Bohman and H. O. G. Siegbahn, *Chem. Phys. Lett.*, 1992, **189**, 414–419.
35 G. Law, P. R. Watson, A. J. Carmichael and K. R. Seddon, *Phys. Chem. Chem. Phys.*, 2001, **3**, 2879–2885.
36 G. Andersson, H. Morgner and K.-D. Schulze, *Nucl. Instrum. Methods Phys. Res., Sect. B*, 2002, **190**, 222–225.
37 G. Andersson and H. Morgner, *Surf. Sci.*, 1998, **405**, 138–151.
38 G. Andersson and H. Morgner, *Surf. Sci.*, 2000, **445**, 89–99.
39 H. Niehus, W. Heiland and E. Taglauer, *Surf. Sci. Rep.*, 1993, **17**, 213–303.
40 G. Andersson and H. Morgner, *Nucl. Instrum. Methods Phys. Res., Sect. B*, 1999, **155**, 357–368.
41 O. A. Baschenko, *J. Electron Spectrosc. Relat. Phenom.*, 1991, **57**, 297–305.
42 O. A. Baschenko and A. E. Nesmeev, *J. Electron Spectrosc. Relat. Phenom.*, 1991, **57**, 33–46.
43 F. Eschen, M. Heyerhoff, H. Morgner and J. Vogt, *J. Phys.: Condens. Matter*, 1995, **7**, 1961–1978.
44 R. Hesse, www.uni-leipzig.de/∼unifit, version 2008.
45 C. Malitesta, I. Losito, L. Sabbatini and P. G. Zambonin, *J. Electron Spectrosc. Relat. Phenom.*, 1995, **76**, 629–634.
46 A. Sanmartín Pensado, P. Malfreyt and A. l. A. H. Pàdua, *J. Phys. Chem. B*, 2009, **113**, 14708–14718.
47 H. Morgner, K. Richter and M. Wulf, *Mol. Phys.*, 1993, **79**, 169–177.
48 J. Günster, O. Höfft, S. Krischok and R. Souda, *Surf. Sci.*, 2008, **602**, 3403–3407.
49 R. M. Lynden-Bell and M. Del Pópolo, *Phys. Chem. Chem. Phys.*, 2006, **8**, 949–954.

 This journal is © the Owner Societies 2010